Electronic Supplementary Material (ESI) for Nanoscale.
This journal is © The Royal Society of Chemistry 2017

Multiple polarization states in symmetric ferroelectric heterostructures for multi-bit non-volatile memories. Electronic Supplementary Information

Georgia A. Boni,[a] Lucian D. Filip,*[a], Cristina Chirila, [a] Iuliana Pasuk,[a] Raluca Negrea, [a] Ioana Pintilie,[a] and Lucian Pintilie[a]

Received Xth XXXXXXXXXX 20XX, Accepted Xth XXXXXXXXX 20XX
First published on the web Xth XXXXXXXXXX 200X
DOI: 10.1039/b000000x

Here we report a ferroelectric capacitor structure obtained by alternating ferroelectric and insulator thin-film layers which allows an increase of up to 2^n polarization states, with n the number of ferroelectric layers. Four and up to eight distinct, stable and independently addressed polarization states are experimentally demonstrated in this work. The experimental findings are supported by a theoretical model based on the Landau-Ginzburg-Devonshire theory. The key parameter is the change in the strain conditions of ferroelectric layers induced by the insulating separator. Notably, the 2^n increase in the storage capacity can be achieved without major changes in the present technology used for FeRAM devices. The test structures demonstrate very good memory characteristics such as retention and fatigue, opening the way towards the design of high density ferroelectric memories.

Four samples based on a ferroelectric-insulator architecture, have been fabricated on $SrTiO_3$ (100) substrate and a 20 nm $SrRuO_3$ electrode. The following naming convention will be used to identify each sample:

1. PZT(150 nm)/STO(5 nm)/PZT(150 nm) = ML1
2. PZT(150 nm)/STO(20 nm)/PZT(150 nm) = ML2
3. PZT(150 nm)/STO(50 nm)/PZT(150 nm) = ML3
4. PZT(100 nm)/STO(10 nm)/PZT(100 nm)/STO(10 nm) /PZT(100 nm) = ML4

The X-ray diffraction (XRD) analysis (Fig. S1) confirms the epitaxial growth of PZT over the entire interface area and throughout the thickness of the films. The analysis revealed differences in the atomic structure of PZT related to the different STO thicknesses and film architectures. These were compared to a regular PZT(100 nm)/SRO(20 nm)/STO substrate heterostructure used as a benchmark, which will be referred to as regular layer (RL).

The XRD patterns of all samples are very consistent, and similar to that of the RL sample. There are two PZT phases with distinct lattice parameters in each system. The analyses of the symmetric $2\theta-\omega$ scans (Fig. S1a)) and of the asymmetric reciprocal space mappings (RSM) (Fig. S1b)) indicate that besides a majority PZT phase characterized by an almost relaxed structure ($a = 3.954$ Å, $c = 4.132$ Å, $c/a = 1.045$) there is a small amount (with intensity approx. ten times less) of almost fully strained phase ($a = 3.914-3.917$ Å, $c = 4.194-4.210$ Å, $c/a = 1.071-1.076$). The strained PZT is thought to be a thin layer at the bottom of the first PZT layer (which is also confirmed by the low magnification TEM images further presented). A structural model where PZT grows strained near the bottom SRO electrode interface, and relaxed on the STO thin film layer, is strongly supported by results obtained on the test samples PZT(150 nm)/STO(20 nm)/SRO(20 nm)/STO substrate (which will be referred to as TS1), which presents a totally relaxed PZT thin film, compared with the case of the test half deposition sequence STO(20 nm)/PZT(150 nm)/SRO(10 nm)/STO substrate (which will be referred to as TS2) or simple RL substrate samples (see Fig. S1c)).

The alignment dispersion of the normals to the PZT (001) planes, obtained by rocking curves on PZT (004) lines is of 0.5° for the relaxed PZT, and of 0.3°–0.4° for the strained one (Fig. S1d)). The rocking curves obtained for the relaxed PZT can be decomposed into two curves with different widths, indicating that one PZT layer is more aligned than the other, with respect to the strained PZT. It is possible that the less aligned PZT layer is the one deposited over the STO interlayer. The presence of STO layer(s) appears to be detectable by their contribution to the shape of the rocking curves obtained on STO (002) (Fig. S1c) to e)). The rocking curve of

[a] *National Institute of Materials Physics, Atomistilor str. 405A, PO Box MG7, Magurele, 077125, Ilfov, Romania; E-mail: lucian.filip@infim.ro*

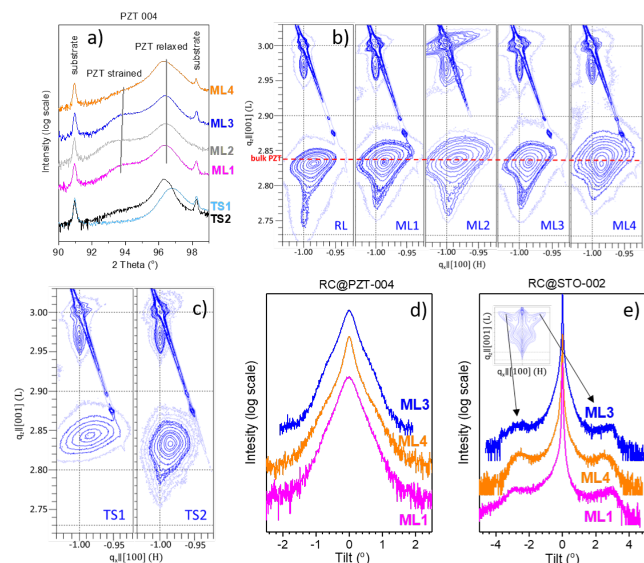

Fig. S1 XRD characterization of the FE-insulators heterostructures: a) $2\theta - \omega$ scans around the (004) line of PZT; b) RSMs near the -103 node of STO; c) RSMs near the -103 node of STO for TS1 and TS2; d) rocking curves on PZT (004) lines; e) rocking curves on STO (002) lines, with RSM around STO (001) (inset).

the STO substrate become wider at the base, when the thickness of the STO layer increases. One can therefore deduce that this widening is a result of the superposition of the much wider and weaker curve of the STO film, which becomes more detectable for thicker films. The shoulders on both sides of the STO rocking curves are the contribution of the rocking curves of the tilted PZT a-domains (see Fig. S1e) inset). It is known that epitaxial PZT relaxes over 100 nm thickness by tilted a-domains [1].

Conventional TEM images presented in Figs. S2 and S3 show the ML4 and ML3 heterostructures respectively. The selected area electron diffraction (SAED) pattern corresponding to the TEM image reveal the epitaxial growth of the constitutive thin layers. Sharp interfaces can be observed between them and also that the surface of the PZT has a low roughness. The strong contrast from the TEM image at the bottom electrode SRO-PZT interface and inside of first PZT layer suggests a high level of strain field in this area. HRTEM images (1) and (2) reveal the PZT-STO interlayer interfaces recorded on the areas inside the red squares from the TEM image.

Both XRD and TEM characterization confirm the epitaxial relation between the layers and the substrate, and similar structure quality with a simple PZT layer deposited on the SRO/STO substrate. It follows that the multi-step polarization switching in the hysteresis cycle measured for these structure has its origin in the electrostatic differences introduced by the

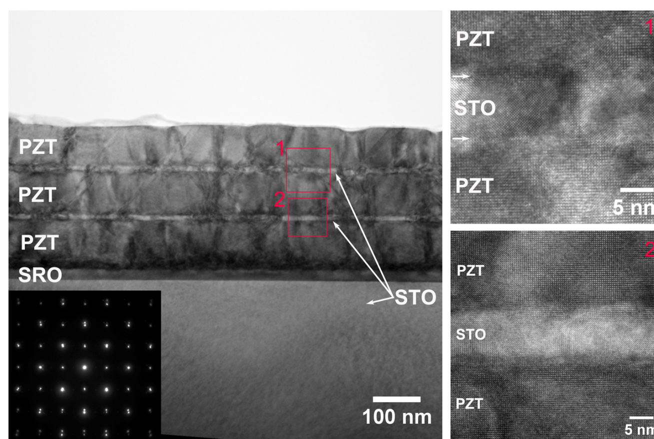

Fig. S2 TEM image at low magnification of the ML4 heterostructure (inset - SAED pattern showing the epitaxial growth of the thin layers on STO substrate) and (1), (2) HRTEM images at PZT/STO/PZT interfaces recorded in the areas inside of red squares from TEM image.

presence of the STO interlayers which induce a perturbation of the potential energy in the structure by comparison to regular PZT based heterostructures. This conclusion is in good agreement with the phenomenological thermodynamic theoretical model used to explain the hysteresis loops, which leads to different strain related parameters for the two ferroelectric layers. This is also observed experimentally since the strain in the PZT layer deposited on the bottom SRO electrode is considerably different than the strain in the PZT layer deposited on the STO interlayer.

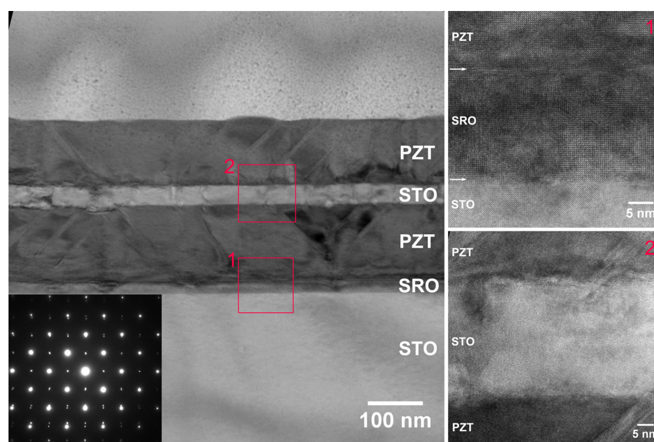

Fig. S3 TEM image at low magnification of ML3 heterostructure (inset - SAED pattern showing the epitaxial growth of the thin layers on STO substrate) and (1), (2) HRTEM images at PZT/SRO/STO and PZT/STO/PZT interfaces recorded in the areas inside of red squares from TEM image.

This journal is © The Royal Society of Chemistry [year]

The ability to maintain a certain polarization state for as long as possible is a qualitative description of non-volatility and it is measured by the retention time of different polarization states (Fig S4). The standard retention measurement is performed by setting one of the four polarization state by using different amplitude of half pulse sequence (see Fig. 2a in the main manuscript)). A read-pulse with the same amplitude as the writing pulse is applied after certain period of time (retention time). During the read pulse, the recorded current will be a combination of dielectric displacement and leakage currents which are the usual expected components. In addition, there will be a back-switching current component also, that occurs during the retention writing time. The retained values of all polarizations are obtained by subtracting the read charge from the written charge ($Q_{retained} = Q_{written} - Q_{read}$). This sequence is repeated with different retention times (up to 10^6 s which is approximatively 2 weeks) for all polarization states.

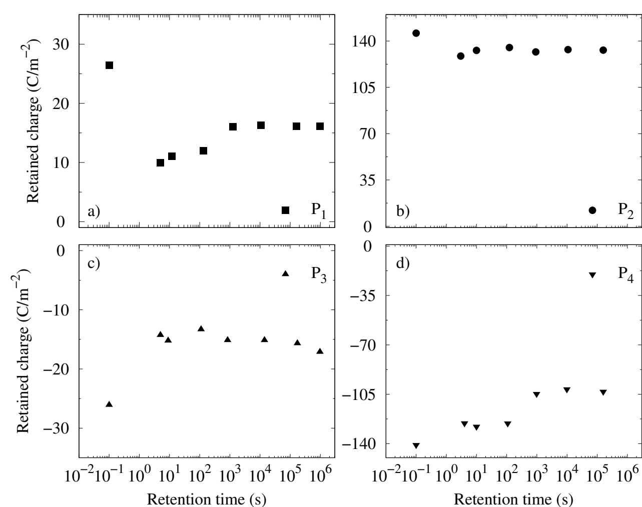

Fig. S4 Retention measurement results for different polarization states; a) P1; b) P2; c) P3; d) P4.

It is a known experimental fact that, over time, the ferroelectric hysteresis could degrade after repeated voltage cycles and characteristics such as the coercive voltages, imprints or doubling of the switching peaks may be modified after operating the memory for a long time. Fatigue measurements have been performed by applying consecutive 25 V voltage full-sequence (dynamic mode) and a number of hysteresis measurements have been recorded at set intervals. In Fig. S5b) and c), all four current switching peaks in the hysteresis show no modification between the first and the 3×10^6th cycle. Only the amplitude values of the current peaks and corresponding polarizations have increased as the number of repetition cycles is increased. This effect can be explained by the possible domain formation and domain pinning centers appearing after the deposition and annealing process, due to the insulator interfaces inside the ferroelectric structure. At the beginning, the FE areas do not respond to the electric stimulus, which determines a decrease of the total polarization compared to the case of a simple ferroelectric layer in contact with conductive electrodes. Considering the high voltage applied during the fatigue operation, the stability of the samples for millions of cycles is outstanding. After 3×10^6 cycles catastrophic degradation takes place suddenly due to an abrupt increase of the leakage current. This is not necessarily a degradation of the structure but rather a degradation of the electrode, which appears to overheat prior to breakdown.

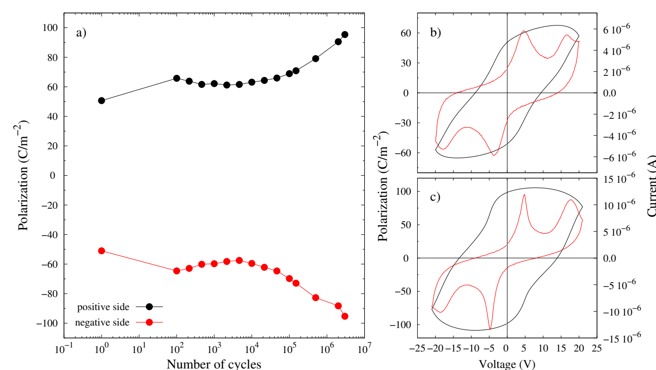

Fig. S5 Fatigue measurement results: a) Evolution of polarization values after repeated number of full voltage sequences; b) Polarization (black line) and Current (red line) hysteresis characteristics after the first voltage pulse; c) Polarization (black line) and Current (red line) hysteresis characteristics after 3 million voltage pulses.

The theoretical model used to corroborate the experimental findings uses a set of fitting parameters that were modified such that a qualitative fit was obtained for the experimental data. The values of the parameters corresponding to the structure sketched in Fig. S6 and used to obtain Figure 3 in the main manuscript are given in Table 1. The values for the β expansion coefficients in the LGD formalism are different which accounts for the deference between the two strain levels in the ferroelectric layers. This is in accordance with the TEM findings and shows that the multi-polarization states appear when the two ferroelectric layers have different strains due to the fact that they are deposited on different substrates (first layer on the conductive SRO, second on the insulating STO). The numerical values for the parameters are in the same range as the ones used in the literature, however they are not intended to carry a specific physical meaning at this stage. Given the simplicity of the proposed theoretical model, even precise values obtained through a rigorous fitting procedure of the experimental data should not be used for a quantitative analysis. The values in Table 1 are given for the purpose of reproducing the

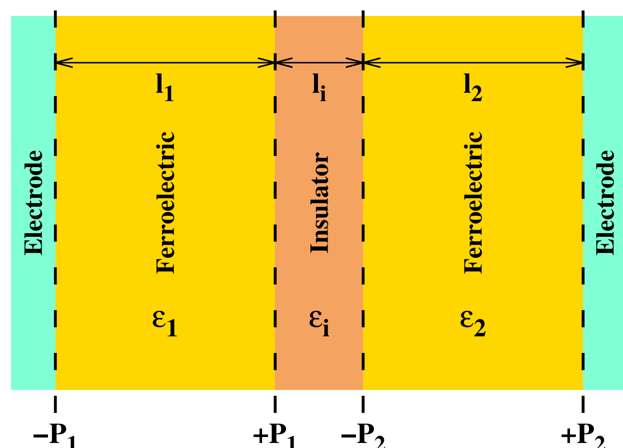

Fig. S6 Schematic of the ferroelectric-insulator-ferroelectric heterostructure. The dotted lines mark the charged sheets used to approximate the polarization in each ferroelectric layer.

Table 1 Numerical values of the fitting parameters used in Equation 7 of the theoretical model in the main text

	First FE layer	Insulator	Second FE layer
dielectric constant	600	100	600
layer width	150 nm	15 nm	150 nm
α	-6.8×10^{8} J m C^{-2}	-	-6.8×10^{8} J m C^{-2}
β	3.5×10^{10} J m^{5} C^{-4}	-	6.5×10^{9} J m^{5} C^{-4}

results. Also, Figure 4 in the main manuscript was obtained by using the same data from Table 1, except that this time the β value of the second layer was the same as the one for the first layer.

Figure 1a) in the main manuscript, shows the influence of the insulator layer thickness on the multi-polarization states. If the insulator thickness is reduced beyond a critical value, the effect disappears since the insulator is no longer capable of maintaining the two ferroelectric layers independent of each other. The same effect can be obtained from the proposed theoretical model and it is shown in Fig. S7.

It can be observed that while it appears that the peaks are better separated for thicker insulator layers, the values of the applied potential where each polarization switch takes place are also increased. This may lead to device failure since a high value for the applied voltage may lead to local overheating of the electrodes or other catastrophic events. An optimum value for the insulator layer thickness is therefore needed in order to balance the multi-polarization state effect and device stability.

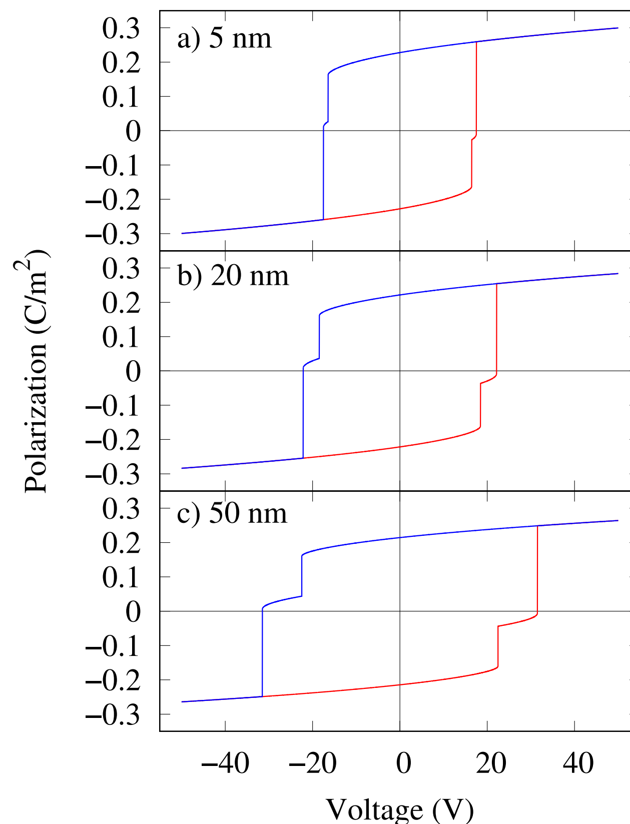

Fig. S7 Hysteresis cycles for different insulator layer thicknesses: a) 5 nm, b) 20 nm and c) 50 nm.

References

1 H. Han, K. Lee, W. Lee, M. Alexe, D. Hesse and S. Baik, *J. Mater. Sci.*, 2009, **44**, 5167–5181.

This journal is © The Royal Society of Chemistry [year]